Spring 2012

Characterizing Electrons in Primary and Secondary Magnetic Islands During Magnetic Reconnection

Jason Shuster
University of New Hampshire - Main Campus

Characterizing Electrons in Primary and Secondary Magnetic Islands During Magnetic Reconnection

Jason Shuster[1]

Advisors: Li-Jen Chen and Roy Torbert
Co-advisor: Harald Kucharek

[1]Department of Physics – University of New Hampshire
Honors Undergraduate Thesis

May 16, 2012

Abstract

The physics underlying particle-in-cell simulations that are widely employed in studying plasma dynamics are reviewed. Results from a two-dimensional particle-in-cell simulation of fully kinetic, undriven, collisionless magnetic reconnection are studied to compare the electrons in a primary magnetic island formed from an ion current sheet and the electrons in a secondary island formed in an electron current layer. We find that the secondary island is born with a strong out-of-plane current density due to localized peaks in the electron density and out-of-plane electron velocity; the secondary island retains these features as it evolves, distinguishing it from the primary island. For the first time distinct features in electron velocity distributions are established for both types of islands. These magnetic island comparisons and their connection to in situ Cluster observations are analysis techniques valuable to NASA's Magnetospheric Multiscale mission to launch in 2014 which is capable of resolving the various types of electron distributions discussed in this thesis.

1 Prologue

Two Courses by which a Scientist Seeks to Acquire Understanding: Observation and Theory

There are two courses by which one may discover new physics underlying physical phenomena: *observation* and *theory*. We understand the process of observation intuitively, for our senses stream observation data to us during every conscious second we have been given, allowing us to make decisions and predictions to aid us in our lives. Theory is a more abstract way of making progress toward understanding, one that exploits the consistencies and patterns that abound in our universe. In a sense, it is still based on observation – just *past* observation instead of present, to-the-minute streaming, in situ (in situation) measurements provided by our senses or instruments. We have the capability to generalize and make abstractions in order to classify and characterize phenomena that we observe. We do this with the assumption that our observations will enable us with a predictive capability which will, in turn, likewise help us make decisions on a day to day basis. These powerful techniques of using present- and past-observations in order to identify patterns about the world around us is the essence of science. At the root of this practice is the fundamental assumption that it is safe and reasonable to suspect that our world is at all times predictable and consistent; yet this assumption we accept in order to make progress. Science does not prove in the sense that mathematics does; yet science represents the bridge, built using the tools of mathematical reasoning, where our desires to seek, classify, and order patterns that we observe meet the physical reality that is our universe.

Just as science is fueled by present in situ measurements combined with the patterns and generalizations made by theoretical observations, these two courses of developing understanding are clearly distinguished in space science as well. In the context of magnetic reconnection, there are still two approaches: one may go for in situ observations, or one may use the predictive capability of theory. For this research study, the author spent the most energy learning how to make strides from a theoretical framework. Specifically, the theoretical tool employed was what is known as a particle-in-cell (PIC) simulation. PIC simulations combine such theoretical pillars as Newton's laws of motion and Maxwell's equations of electromagnetism with numerical computation in order to study plasma dynamics. The objective of the research was to use results from a PIC simulation to characterize electrons in two-dimensional (2D) magnetic islands formed during magnetic reconnection. As the author gained familiarity with this simulation and was able to make conclusions concerning these simulation results, he was able to qualitatively compare these results with the analogous data from in situ measurements made by the four Cluster spacecraft, successfully launched and operational since the summer of 2000.

This work has sparked a passion within the author that leads him to pursue graduate study in this same field of space science. It has been an extremely rewarding experience for the author to commence work over a year and a half ago in a field about which he knew very little, and to progress to a point where his research is at the frontier of the field. He is learning to bridge the theoretical and observational aspects of space science in order to take steps toward understanding the mysteries of magnetic reconnection.

2 Introduction

The following section addresses basic questions to provide an introduction to the concepts of magnetic reconnection, magnetic islands, and PIC simulations.

2.1 What is magnetic reconnection?

While to some the phrase "magnetic reconnection" may seem too complicated to understand, odds are that many have seen a kind of "reconnection" before without even realizing it. Aircraft contrails (or vortex trails) actually experience the same kind of "reconnecting" motion that magnetic field lines undergo in the process of magnetic reconnection. The similarity between these two physical phenomena implies the existence of a formal similarity between the mathematics used to describe these two processes. The vorticity equation governing contrails is, in fact, identical to the magnetic field equation governing magnetic reconnection if the vorticity is replaced by the magnetic field [1]. Though there are many other complexities that arise in the context of plasma dynamics when explaining magnetic reconnection, many of the contrails can be seen to "reconnect" and pinch together downstream from the jet engines producing them. Seeing such readily visible evidence

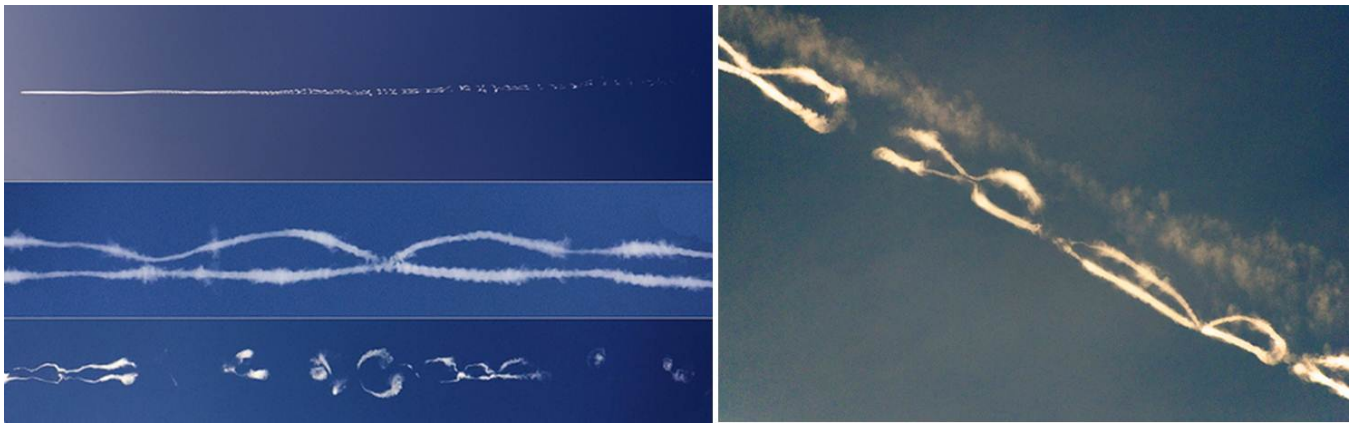

Figure 1: Images of aircraft contrails merging in a similar fashion to the way in which magnetic field lines 'reconnect' to form magnetic islands [6].

of similar phenomenological processes of nature is inspiring to the author, who enjoys sharing his excitement with friends inquiring about his research by pointing overhead at the reconnecting contrails of an airplane and saying: "Look: *reconnection*!"

Magnetic reconnection is a fundamental energy conversion process. Physics tells us that energy is neither created nor destroyed – rather, energy may be *converted* into many different forms. The kinetic energy stored in a moving vehicle is converted to heat through the process of friction when brakes stop a car. Similarly, magnetic energy stored in magnetic fields is converted to plasma kinetic energy and heat through the process of magnetic reconnection. However, magnetic reconnection is still not fully understood. This is to say that we have not been able to explain through observation or theory just how this energy conversion process of magnetic reconnection works.

We research reconnection with this hope: to be able to explain and understand the underlying physical mechanisms that enable it. The sole purpose of the National Aeronautics and Space Administration's (NASA) flagship mission, Magnetosphereic Multiscale (MMS), in which UNH plays a leading role, is to discover the microphysics of magnetic reconnection in the magnetosphere [2]. Applications of magnetic reconnection include: solar dynamo theory concerning the generation of magnetic fields in planets and stars, thermonuclear fusion in which extremely intense magnetic fields are used in devices called tokamaks to confine plasma in hopes of harnessing energy in a similar fashion to the way in which our own sun produces energy, and the production of the northern and southern lights (aurorae) as reconnection occurs in the Earth's magnetotail region of our magneto-

sphere to release energetic particles that stream along our planet's magnetic field and bombard our atmosphere.

For this thesis, the author studies magnetic reconnection as it applies to space plasmas and specifically plasmas in the Earth's magnetosphere. Figure 2 shows a depiction of reconnection as it occurs in the magnetotail region of the Earth's magnetosphere. To conduct this study, we

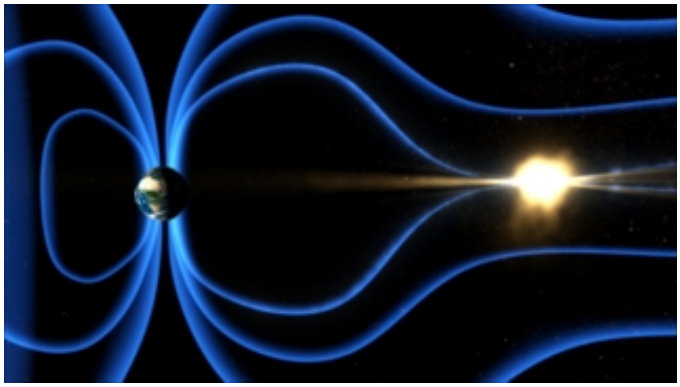

Figure 2: Depiction of magnetic reconnection releasing energy in the Earth's magnetotail [3].

use results from a highly sophisticated PIC simulation run on a supercomputer at Los Alamos. This simulation tracked over one and a half billion particles in order to simulate the behavior of plasma before and after reconnection was initiated. The goal of this research study is to characterize electrons in magnetic islands that form during reconnection. Magnetic islands are known to be linked to the energization of particles in the Earth's magnetosphere [4]. Understanding the dynamics of electrons within these islands is a step closer toward understanding the underlying physics of magnetic reconnection itself.

2.2 What are magnetic islands?

Simply stated, magnetic islands are closed loops in the topology of a magnetic field. These islands (also known as plasmoids) in two dimensions (2D) are believed to be cross sections of "flux ropes" which have been observed in three-dimensional studies of magnetic reconnection. Islands are the result of two reconnection X-lines which form and bound a region of plasma. An X-line is a feature of the magnetic field topology which characterizes the notion of "reconnection." It occurs when oppositely directed fields are compressed to the point where they effectively 'break' and 'reconnect' (see Figure 3). In this process of active reconnection, two exhaust regions form as plasmas are ejected outward away from the diffusion region at the reconnection site. Magnetic islands may form when multiple X-lines develop. In the region bounded by two X-lines, the magnetic field lines form closed loops. This region of plasma with closed loops in the magnetic field is what is referred to as a magnetic island (see Figure 4). Plasma outflow jets from the exhaust regions of the bounding reconnection X-lines collide in this island region. An island may grow in size, like an inflating balloon, as plasma piles up inside the island.

The descriptors "primary" and "secondary" are used to differentiate between the formation of these different islands; the primary island develops from the ion current layer with a spatial scale on the order of an ion skin depth (d_i), whereas the secondary island is born from the electron current layer with a spatial scale on the order of an electron skin depth (d_e) (see Figure 4). A "skin depth" is a length which measures how far electromagnetic radiation is able to penetrate into matter [7]. An

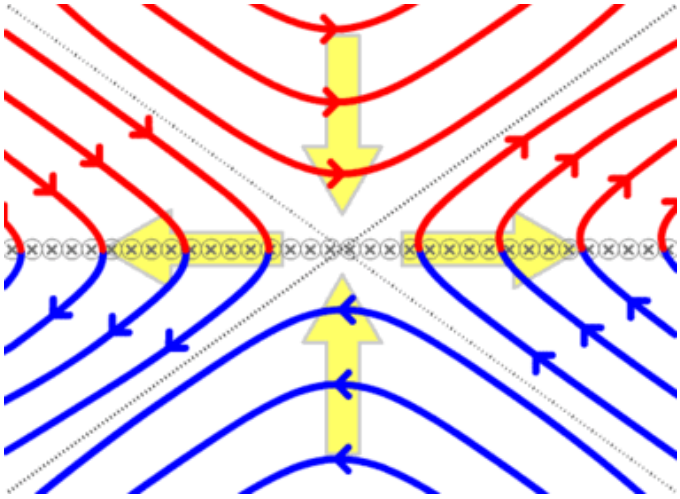

Figure 3: Schematic illustrating the way in which oppositely directed field lines pinch together and reconnect in an X-like configuration [8].

ion skin depth is c/ω_{pi}, where c is the speed of light and ω_{pi} is the ion plasma frequency. An electron skin depth is c/ω_{pe}, where again c is the speed of light, and ω_{pe} is the electron plasma frequency. These frequencies are the frequencies at which ions and electrons oscillate in a plasma. Plasma oscillations are important for describing the temporal and spatial scales of reconnection. Plasma oscillations occur as negatively charged electrons and positively charged ions move in response to electric fields. The electrons and ions will initially accelerate so as to cancel any electric fields that develop within the plasma. Then, once the field is balanced, like charges will repel one another; electrons will repel electrons, and ions will repel ions. The resulting motion is an oscillation of the plasma which occurs at the *plasma frequency*. Another useful frequency commonly used to measure the time scale of PIC simulations is the cyclotron frequency, Ω (also known as the gyrofrequency). The electron cyclotron frequency, Ω_{ce}, and the ion cyclotron frequency, Ω_{ci}, are the frequencies at which electrons and ions gyrate in the presence of a magnetic field. This gyration is a circular motion in the plane perpendicular to the direction of the magnetic field.

State of Knowledge Concerning Magnetic Islands Before This Work

Before this work, electron distributions in both islands and exhaust regions were thought to be hot and fairly isotropic without much structure [4], [5]. This study was carried out to attain a deeper understanding of the dynamics and behavior of electrons in both primary and secondary magnetic islands that form in this PIC simulation (see Figure 4). As a result, this work reveals there to be many more complexities in the structure of electrons within islands and exhaust regions than was previously thought. This work's importance stems from its contribution to furthering our knowledge of electron kinetic physics in magnetic islands. This knowledge is needed in order to fully understand the role islands play in reconnection dynamics, such as electron acceleration, nonlinear wave generation [9], and how islands may facilitate fast reconnection [10], [11].

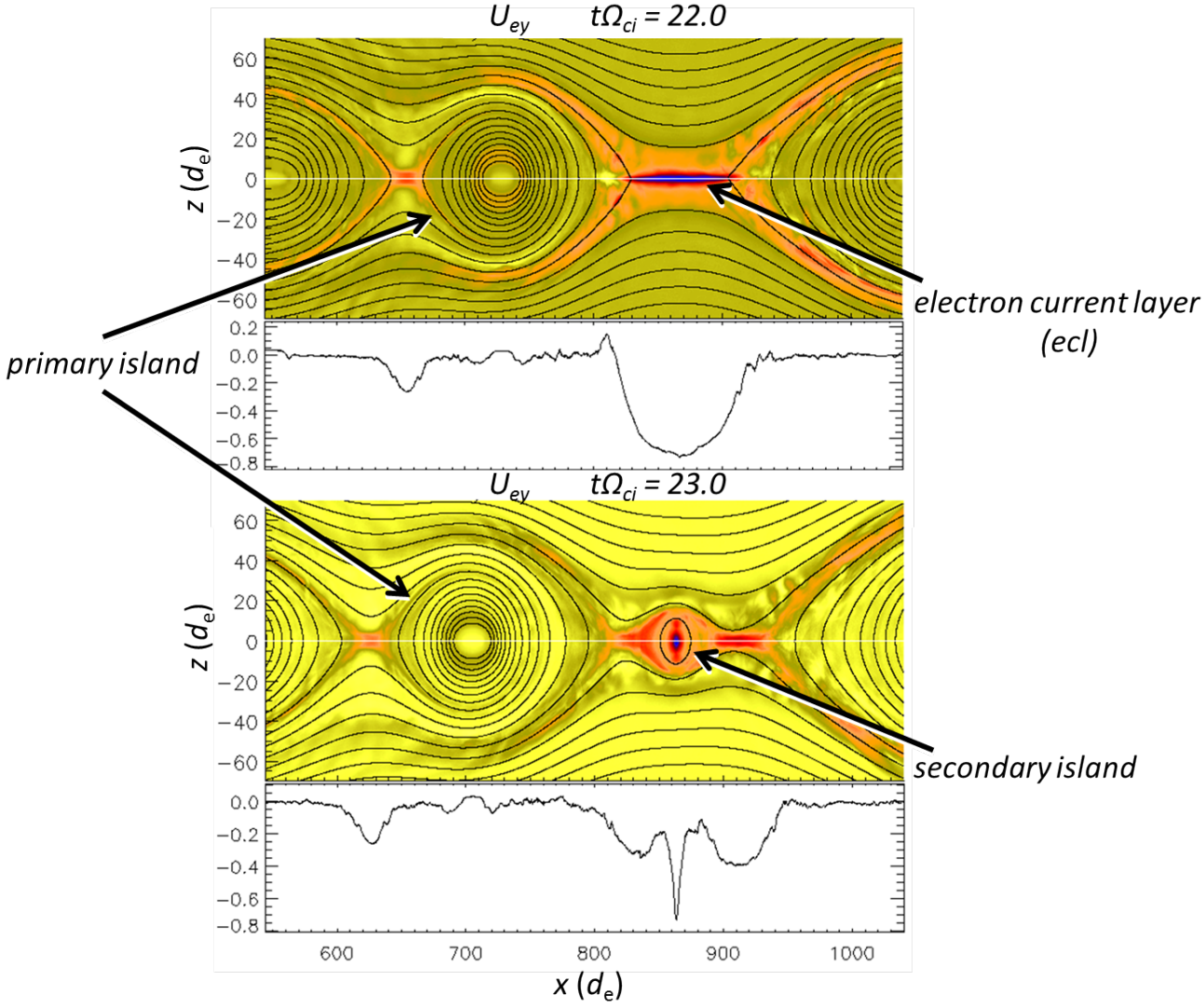

Figure 4: Plots of the out-of-plane electron velocity, U_{ey}, from $t\Omega_{ci} = 22.0$ just before (top) and $t\Omega_{ci} = 23.0$ just after (bottom) the birth of the secondary island. $+x$ denotes the horizontal distance from left to right, $+y$ denotes the direction into the page, and $+z$ denotes the vertical distance from bottom to top. The background contours represent the magnetic field lines in the x-z plane. From the time before the birth of the secondary island, a cut across the data at $z = 0$ shows the region of strong electron flow at the electron current layer (*ecl*). From the time just after the birth of the secondary island, this peak in the out-of-plane electron flow feature is preserved at the island's core, distinguishing it from the primary island whose core shows no such feature.

2.3 Particle-in-Cell Simulations

Plasma physicists widely use particle-in-cell (PIC) codes to model plasmas. A plasma is defined to be an ionized gas, so that while the fluid dynamics used to describe the air in a room or the water in a vortex are needed, electromagnetism is also required to describe the behavior of the charged particles which comprise the plasma. The traditional theory developed to combine these theories is Magnetohydrodynamics (MHD). While adequate on a larger, global scale, MHD is destined to

fail in regions at boundary regions such as the magnetopause where reconnection is known to occur [12]. This is where PIC codes become advantageous. They work well to better describe the kinetic effects of particles within plasmas. To do this, there is a cost – highly sophisticated PIC codes are expensive computationally, for they track on the order of a billion (10^9) or even a trillion (10^{12}) individual particles. The physical theory underlying PIC simulations is simply Newton's Laws of motion,

$$m\frac{d\mathbf{v}}{dt} = \mathbf{F} = q(\mathbf{E} + \mathbf{v} \times \mathbf{B}) \tag{1}$$

$$\frac{d\mathbf{x}}{dt} = \mathbf{v} \tag{2}$$

and Maxwell's equations of electromagnetism,

$$\frac{\partial \mathbf{E}}{\partial t} = \frac{(\nabla \times \mathbf{B})}{\mu_o \epsilon_o} - \frac{\mathbf{J}}{\epsilon_o} \tag{3}$$

$$\frac{\partial \mathbf{B}}{\partial t} = -(\nabla \times \mathbf{E}). \tag{4}$$

These equations are used to advance the velocity and position of each particle in time. During the simulation run, this information is used to determine the current density and plasma density, which is in turn used to calculate the electric field, **E**, and the magnetic field, **B**, as well as other useful quantities such as the plasma pressure tensor components.

2.3.1 PIC History and Limitations

The PIC technique developed as a less computationally intensive method compared to calculating the Coulomb force on particles due to all surrounding particles. Calculating the Coulomb force for every particle in this way as was done in early plasma simulations is very limiting because it means that the number of computations needed for the simulation scales as the square of the number of particles, N. This N^2 dependence renders it impossible to use a realistic number of particles to model a plasma. The "particle-in-cell" technique instead calculates the fields and other bulk quantities for individual cells of an overlaid spatial grid, and then uses an interpolation scheme to interpolate back for particles within each cell [12]. This technique reduces the number of computations needed from N^2 to $NlogN$.

In PIC simulations modeling plasma, the length of time needed to run the simulation is sensitive to the mass ratio of the plasma species in question. For the simulation discussed in this thesis, there are only two plasma species: protons (positively charged, H^+ ions) and electrons. The true mass ratio between a proton and an electron is: $m_i/m_e \approx 1836$. In order for the time required to run the simulation to be practical, often artificial mass ratios are used to balance strict temporal and spatial constraints needed to properly model the underlying physics. One condition, as a consequence of Ohm's Law, is the Courant-Friedrichs-Lewy (CFL) condition. This is a requirement that the distance a wave travels in one time step must be smaller than the grid spacing used in the simulation [12]. The PIC simulation discussed in this study uses $m_i/m_e = 400$.

2.4 Electron Velocity Distribution Functions

In this study, the main representation used to examine the structure of electrons are electron velocity distribution functions (also referred to as electron velocity distributions). An electron distribution in

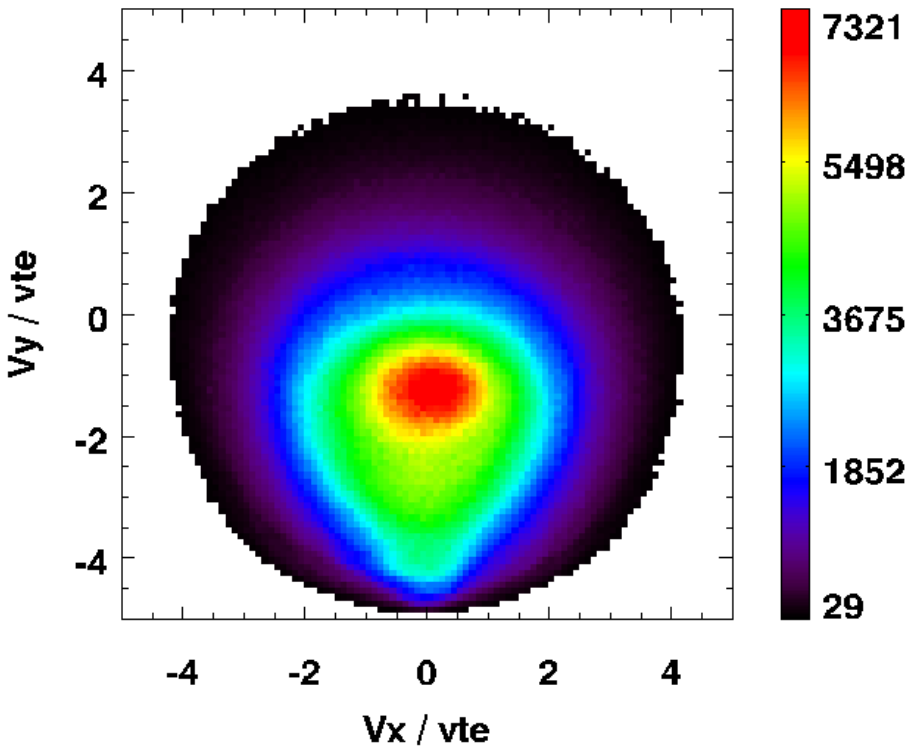

Figure 5: An example of an electron distribution function in velocity space. This representation is a two dimensional histogram, where the color represents the number of electrons that have the particular velocities as indicated by the two axes. This electron distribution function was created using a large spatial bin size encompassing the entire secondary island from $t\Omega_{ci} = 23.0$ ($x = [840, 880]d_e$ and $z = [-10, 10]d_e$, see Figure 4).

velocity space (see Figure 5) shows a two-dimensional histogram of the velocities of all the electrons in question. As an analogy, one might consider the velocity distribution of air molecules in a room, the velocity distribution of water molecues in a section of a river, or the velocity distribution of particles in some other fluid context.

The electron velocity distributions studied in this work are effective snapshots of the electrons in velocity space from a specified region of the PIC simulation domain. These distributions are produced using the full particle data, and so they offer a thorough understanding of electron motion which may be lost when looking at averaged data, such as the velocity data shown in Figure 4. When arranged in an array, multiple distributions can help to construct an effective map of the structure of electrons in an entire region. We use this approach, similar to the "picture-puzzle" approach used with in situ data from the Cluster spacecraft [5], to provide such a map for the electrons in the two magnetic islands of this PIC simulation.

Each distribution function is accumulated by first specifying a particular bin of data from which to construct the distribution. If this bin size is large, such as the bin size used to produce the distribution function in Figure 5, then it becomes difficult to identify the spatial location of the electrons contributing most to the shape of the distribution. For instance, in Figure 5 we see that the distribution is relatively isotropic, but it is significantly skewed in the negative V_y-direction. This indicates that there are a significant number of electrons with large velocities in the negative y-direction. However, the bin size was 20 d_e in z by 40 d_e in x, covering the entire secondary island

region (see Figure 4), so we have no way of knowing where in the island's electrons this strong out-of-plane (y-direction) flow is observed. On the other hand, if the bin is too small, then there would be too few electrons represented to make strong conclusions from the distribution. We determined an appropriate bin size to be 2 d_e by 2 d_e, which represents a spatial area of 4 d_e^2. The distributions shown in the next section (see Figures 6, 7, and 8) are all made using this bin size. The electron velocity distributions studied are normalized by the electron thermal velocity, v_{te}, from the initial Maxwell distribution. The electron thermal velocity is defined as $v_{te} = (kT_e/m_e)^{1/2}$, where k is the Boltzmann constant, T_e is the temperature of the electrons in the plasma, and m_e is the electron mass [13].

3 Results

In the following section, the objectives of this research study are identified. The results of our research as it pertains to these objectives are then presented. We study electron particle data from four evolution stages of reconnection. At the earliest stage, where $t\Omega_{ci} = 17.0$, the primary island has formed due to two X-lines after magnetic reconnection was initiated in the PIC code. At a later stage, when $t\Omega_{ci} = 22.0$, the secondary island is born from the electron current layer (*ecl*). Electron distribution functions are arranged to make an effective map in order to understand the structure and motion of electrons in each of the islands and in the reconnection exhaust region.

3.1 Research Study

3.1.1 Main Objective

The main objective of this thesis is to compare primary and secondary magnetic islands by characterizing electrons in a PIC simulation of 2D magnetic reconnection, and establish for the first time distinct features in electron velocity distributions for both types of islands.

3.1.2 Secondary Objective

The second objective of this thesis is to use the comparison techniques developed for accomplishing the main objective to examine the assumption that electron distributions in the interior of magnetic islands are similar to those in the exhaust reconnection regions. Before this work, electron distributions in both islands and exhaust regions were thought to be hot and isotropic without much structure.

3.2 Simulation Parameters

This PIC simulation models collisionless, undriven reconnection started from an initial Harris current sheet with zero guide field and open boundary conditions. In a Harris current sheet, the magnetic field in the x-direction is given by $B_x = B_0 tanh(z/L)$, where B_0 is the initial upstream magnetic field strength, and L is the half-width of the current sheet (see Figure 4 to see the orientation of the x, y, and z coordinate system). This simulation is two-dimensional (2D), and so there is no variation in the plasma in the y-direction; *i.e.*, all quantities shown in the x-z plane are considered to be uniform in y. The density profile, $n(z)$, for this Harris sheet is $n(z) = n_0 sech^2(z/L) + n_b$, where n_0 is the Harris density and n_b is a uniform background density. The ratio of the thermal pressure to the magnetic pressure, β, is 0.0028, appropriate for modeling plasma in the lobe regions

of the Earth's magnetosphere. β is defined to be $8\pi nkT/B^2$, where n is the number density of the plasma, k is the Boltzmann constant, T is the plasma temperature, and B is the magnetic field strength [13]. The mass ratio of the two plasma species, protons and electrons, is $m_i/m_e = 400$. The ratio of plasma temperatures for the Harris population is $T_i/T_e = 5$. The ratio of the electron plasma frequency to the electron cyclotron frequency is $\omega_{pe}/\Omega_{ce} = 2$, which represents a constraint on the speed of light. The ratio of the half width of the current sheet to an ion skin depth is $L/d_i = 0.5$, or $L = 10\ d_e$. (Because of the artificial mass ratio, m_i/m_e, 1 d_i = 20 d_e.) The ratio of the background density to the initial density is $n_b/n_o = 0.05$. The ratio of the background temperature to the initial temperature is $T_b/T_o = 0.333$. The number of cells in this simulation is 1024×2560 cells and there are 600 particles per cell, so the total number of particles in this simulation is $\approx 1.5 \times 10^9$, over 1.5 *billion* particles.

3.2.1 Primary Island

From the electron distribution maps constructed for the primary island at $t\Omega_{ci} = 23.0$, we see highly structured electron distributions (see Figure 6). A colder, dense core is clearly discernable from the distribution functions that is isotropic in both V_x vs. V_y and V_x vs. V_z velocity space. There is strong heating in the direction perpendicular to the magnetic field (*i.e.* perpendicular heating) in the V_x vs. V_z distributions. Electrons are hottest (largest spread in velocity space) inside the island, just outside the island core. Further away from the island core, we see a new velocity-space-hole structure in the V_x vs. V_y distributions, showing that there is a gap in the electron energies in this region of the island. This new structure coincides with semi-open magnetic field lines of the island. The semi-open field lines are open on the $-x$ side of the island and closed on the $+x$ side due to the faster reconnection rate of the X-line on the $+x$ side of the island. In future work, we plan to develop code to trace particle orbits in this region to help us understand the underlying physics that is captured by these types of distributions.

At the earliest stage, $t\Omega_{ci} = 17.0$, the primary island's electron velocity distributions were fairly isotropic. Nevertheless, even at this early stage we see faint ring-structures in the V_x vs. V_y distributions at the semi-open field-line region with $z = 0$. There are other noticable anisotropies in both V_x vs. V_y and V_x vs. V_z distributions, such as double peak structures indicating counter-streaming electrons near the edges of the island, though these anisotropies are not as prevalent as in later evolution stages, such as at $t\Omega_{ci} = 22.0$, $t\Omega_{ci} = 23.0$ (see Figure 6), and $t\Omega_{ci} = 26.0$.

3.2.2 Secondary Island

From the electron distribution maps constructed for the newborn secondary island at $t\Omega_{ci} = 23.0$, we again see highly structured electron distributions (see Figure 7). Such dynamic electrons are the result of active reconnection. The secondary island has a region towards its edge where three distinct electron populations are visible in the distribution functions, indicating counter-streaming electrons. As with the primary island, we discern a colder, dense island core. However, there is a distinct difference in the secondary island's core in V_x vs. V_y velocity space: it is skewed significantly in the negative V_y-direction. This indicates a strong out-of-plane electron flow in the negative y-direction. The secondary island appears to have retained this feature from the initial peak in the out-of-plane electron flow from the electron current layer from which the island was born (see Figure 4). Even as the secondary island evolves in time throughout the simulation, it retains this feature, distinguishing it from the primary island.

From the two evolution stages studied after the island birth, $t\Omega_{ci} = 23.0$ and $t\Omega_{ci} = 26.0$, electron distribution functions show the development of the colder, denser island core which can be

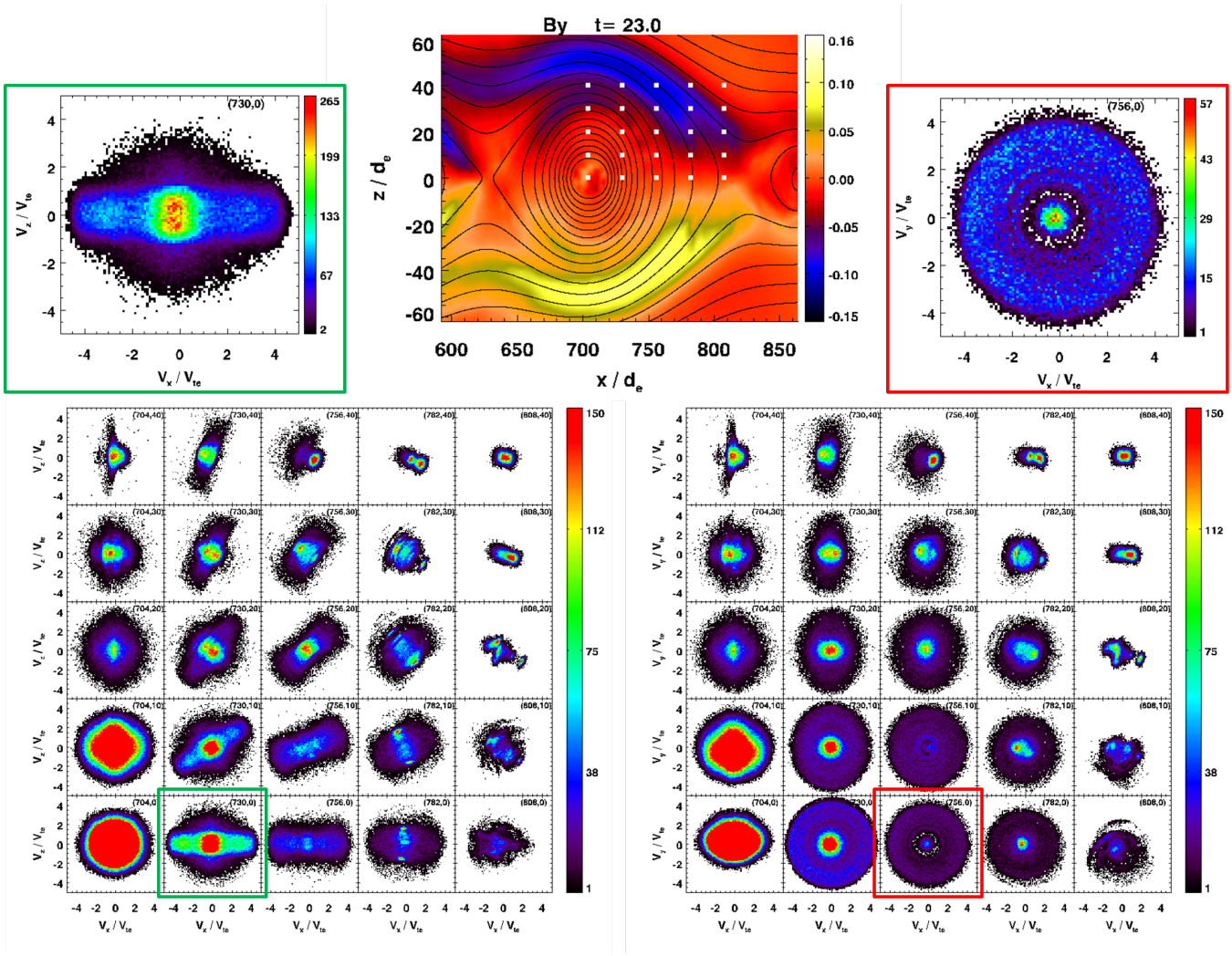

Figure 6: Electron velocity distributions showing the structure of electrons within the primary magnetic island. The uppermost plot shows the out-of-plane magnetic field strength, B_y, of the primary island at $t\Omega_{ci} = 23.0$. The overplotted white grid points represent the to-scale bin sizes and locations chosen to produce the electron velocity distribution arrays shown. The leftmost array of distributions is in V_x vs. V_z velocity space, while the rightmost array of distributions is in V_x vs. V_y velocity space. The green box (upper left) shows a larger view of the perpendicular heating seen in V_x vs. V_z, while the red box (upper right) shows an example of a new velocity-space-hole structure.

seen in both V_x vs. V_y and V_x vs. V_z. The highlight in Figure 7 in red shows a distribution from the secondary island's core at $t\Omega_{ci} = 26.0$, showing the fastest electrons out of all the distribution functions studied. The secondary island grows to d_i scale size by $t\Omega_{ci} = 23.0$. The triple populations, like that shown in the green highlight of Figure 7, become less intense as the island grows, indicating fewer counter-streaming electrons as the island develops.

3.3 Island Regions Compared to the Open Exhaust Regions

Using these electron velocity distributions, we are able to compare the electrons within the islands to the open exhaust regions of the simulation (see Figure 8). Previously, electrons within

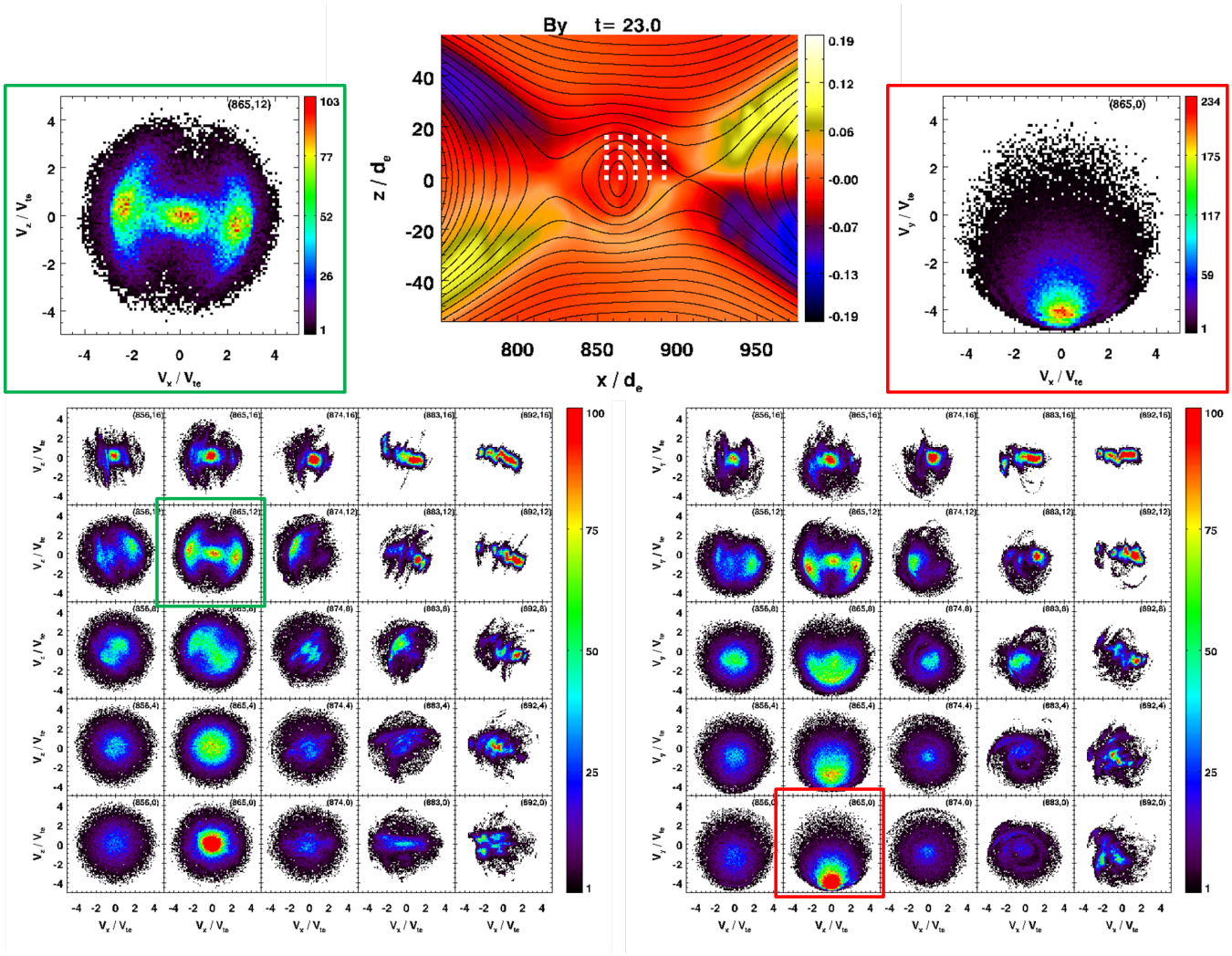

Figure 7: Electron velocity distributions of the secondary magnetic island at $t\Omega_{ci} = 23.0$. The layout of the data in this figure is analogous to that of Figure 6 – each electron velocity distribution in the distribution maps correspond to the to-scale white bins overlaid on the spatial plot of the secondary island above the maps. The distribution shown in the green box (upper left) shows the type of triple populations seen in both V_x vs. V_z and V_x vs. V_y, while the distribution shown in the red box (upper right) highlights the intense out-of-plane electron flow feature unique to the secondary island.

the islands were assumed to be similar to those in the exhaust. We show this assumption to be an oversimplification. Electrons in the exhaust are also highly structured, though they exhibit different anisotropies than the islands. At an early stage of island formation, the exhaust distributions are fairly isotropic, consistent with previous results [5]. At later stages, however, many more complexities develop, such as perpendicular heating at the region of intense magnetic field compression and triple populations distinct from those found in the secondary island.

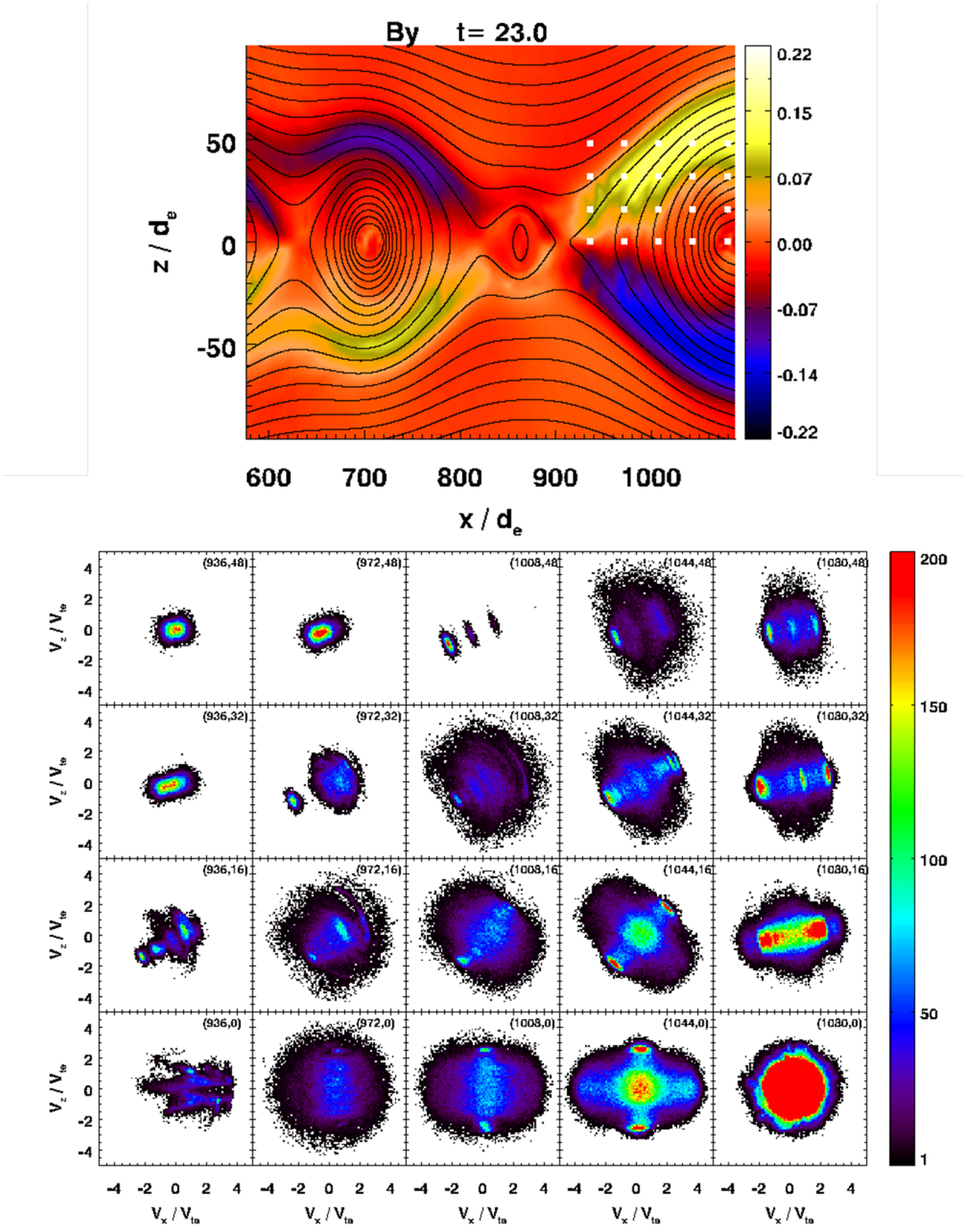

Figure 8: Electron velocity distributions from the open exhaust region at the same time ($t\Omega_{ci} = 23.0$) as the distribution arrays shown in Figures 6 and 7.

3.4 Cluster Data

This study of simulation electron velocity distributions constructs arrays of distributions to map out the island interior and surroundings. A similar approach has been used to successfully reconstruct a view of a magnetic reconnection X-line with electron data in energy space measured by the four Cluster spacecraft [5]. This same X-line region is shown here in velocity space to illustrate the

similarities between actual in situ measurements of electron velocity distributions and the electron velocity distributions produced in this simulation study (see Figure 9).

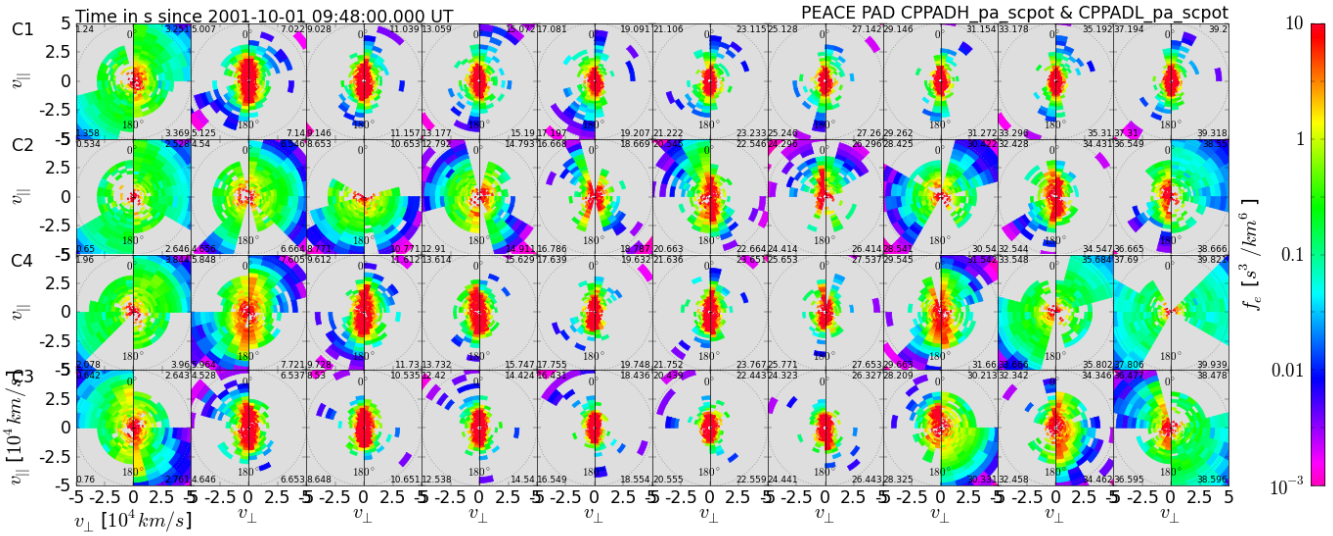

Figure 9: Actual in situ observations of electron velocity distributions from a diffusion region during magnetotail reconnection in the Earth's magnetosphere, observed on 1 October 2001. These distributions were arranged in this way to uncover the X-line topology characteristic of a magnetic reconnection diffusion region [5] (see Figure 3). These Cluster data are compared with Figures 6, 7, and 8 to see how we may make future comparisons between simulations and in situ measurements to further understand magnetic reconnection.

The axes of the distributions shown in Figure 9 are $V_\perp$ and $V_\parallel$, denoting velocities perpendicular ($\perp$) and parallel ($\parallel$) to the direction of the magnetic field. The array of Cluster distribution functions represents a time series with each half-panel showing 2 seconds of data. The Cluster spacecraft spin as they collect data, and the spin period of the spacecraft is 4 seconds so that each square (two half-panels) contains data from an entire 360° rotation.

The narrow, elongated structures seen in the Cluster data are known as *inflow* regions [5]. In these regions, velocity distributions are elongated in the parallel direction, indicating parallel heating as the electrons flow into the diffusion region. We see these same elongated structures in the simulation distributions. The upper rightmost distributions in both V_x vs. V_z and V_x vs. V_y arrays for the secondary island (Figure 7) and the upper leftmost distributions in the open exhaust (Figure 8) show the same elongation in the direction parallel to the magnetic field.

The Cluster distributions towards the left and right of Figure 9 are hotter as can be seen by their larger spread in velocity space. These in situ observations correspond to the hotter simulation distributions within the islands and exhaust regions. Figures 6, 7, and 8 all show hotter distributions compared to colder distributions from outside the islands or exhaust region, just like those seen in the Cluster observations.

NASA's Magnetospheric Multiscale (MMS) mission to launch in 2014 is designed with a resolution capable of revealing the detailed structures we see in these simulation distributions [2]. By using the types of analysis techniques employed in this study with these highly resolved distributions from MMS, we hope to take further steps closer understanding the microphysics of magnetic reconnection diffusion regions.

4 Summary and Conclusions

We successfully employ an analysis technique using electron velocity distributions from PIC simulation results to gain insight into the electron behavior and dynamics within magnetic islands.

A characteristic difference between the primary island and secondary island is observed: the core of the secondary island retains the strong out-of-plane electron flow feature that it acquired from the electron current layer from which it was born, while the primary island core shows no such feature. In addition, velocity-space distribution functions reveal new structures within these magnetic islands: a distinct velocity-space-hole structure only within the primary island; triple populations in the secondary island indicating counter-streaming electrons; elongated structures suggesting differing amounts of parallel and perpendicular heating; ring-resembling structures indicating a gap in electron energies in both islands; the existence of a less energetic, dense electron region at the center of each island.

We also use the analysis technique to check the assumption that island electrons are roughly similar to open-exhaust electrons. We find this assumption to be an oversimplification, only valid at early stages of reconnection.

We hope to extend the analysis techniques used in this thesis to the future results of NASA's Magnetospheric Multiscale (MMS) mission scheduled to launch in 2014. In doing so, we plan to make further strides toward uncovering the mystery of magnetic reconnection.

Acknowledgements

The author wishes to sincerely thank his research advisor, Dr. Li-Jen Chen, for sharing her passion for physics with him; this work could not have been completed without her continued instruction and ongoing support. In addition, the author would like to thank his advisor, Dr. Roy Torbert, for his guidance concerning this work and for his financial support which helped to enable the author to present this research at the 2011 American Geophysical Union (AGU) Fall Conference meeting in San Francisco. Lastly, we would like to thank our collaborator at Los Alomos, Dr. William Daughton, whose simulation data we use to conduct these types of studies.

References

[1] Gurnett, D. A. *Merging of aircraft vortex trails: similarities to magnetic field merging.* Geophys. Res. Lett., Vol. **16**, No. 1, pp.17-20, January 1989.

[2] National Aeronautics and Space Administration (NASA), Goddard Space Flight Center. Accessed: 30 April 2012. http://mms.gsfc.nasa.gov/

[3] Institute for Geophysics and Extraterrestrial Physics. Accessed: 8 May 2012. http://www.igep.tu-bs.de

[4] Chen, L.-J., et al. *Observation of energetic electrons within magnetic islands.* Nature Phys., **4**, pp.19-23, 2008.

[5] Chen, L.-J., et al. *Evidence of an extended electron current sheet and its neighboring magnetic island during magnetotail reconnection.* J. Geophys. Res., **113**, A12213, 2008.

[6] Mitra Images. *Crow Instability.* Accessed: 2 May 2012. http://images.mitrasites.com/crow-instability.html

[7] Griffiths, D. L. *Introduction to Electrodynamics*, 3rd edition. Prentice Hall, 1999.

[8] Wikipedia, *Magnetic Reconnection*. Accessed: 29 April 2012. http://en.wikipedia.org/wiki/Magnetic_reconnection

[9] Khotyaintsev, Y., et al. *Observations of slow electron holes at a magnetic reconnection site.* Phys. Rev. Lett., 105, 165002, 2010.

[10] Shibata, K. and S. Tanuma. *Plasmoid-induced-reconnection and fractal reconnection.* Earth, Planets, and Space, **53**, 473-482, 2001.

[11] Bhattacharjee, A., et al. *Fast reconnection in high-Lundquist-number plasmas due to the plasmoid instability.* Phys. Plasmas, 16(11), 112,102-5, 2009.

[12] Pritchett, P. *Particle-in-Cell Simulations of Magnetosphere Electrodynamics.* IEEE Transactions, **28**, pp.1976-1990, 2000.

[13] J.D. Huba. *NRL Plasma Formulary.* Naval Research Laboratory, pp.28-29, 2007.